eNeuro Accepted Manuscript

eNeuro

*Research Article: New Research | Disorders of the Nervous System*

# Enhanced GABAergic Inputs Contribute to Functional Alterations of Cholinergic Interneurons in the R6/2 Mouse Model of Huntington's Disease

Cholinergic Interneurons in Huntington's Disease

**Sandra M. Holley, Prasad R. Joshi, Anna Parievsky, Laurie Galvan, Jane Y. Chen, Yvette E. Fisher, My N. Huynh, Carlos Cepeda and Michael S. Levine**

*Intellectual and Developmental Disabilities Research Center, Semel Institute for Neuroscience and Human Behavior, University of California at Los Angeles, Los Angeles, CA 90095*

DOI: 10.1523/ENEURO.0008-14.2015

Received: 27 August 2014

Revised: 17 February 2015

Accepted: 20 February 2015

Published: 24 February 2015

**Author Contributions:** S.M.H., P.J., A.P., L.G., J.Y.C., Y.E.F., and M.H. performed research; S.M.H., P.J., A.P., L.G., J.Y.C., Y.E.F., M.H., C.C., and M.S.L. analyzed data; S.M.H., P.J., C.C., and M.S.L. wrote the paper; C.C. and M.S.L. designed research.

**Funding:** NIH
NS41574

**Funding:** Cure Huntington's Disease Initiative (CHDI Foundation)
100006500

**Conflict of Interest:** Authors report no conflict of interest.

Funding was provided by CHDI, Inc. and USPHS NS41574.

**Correspondence should be addressed to** S.M.H. and P.R.J. contributed equally to this work.

**Correspondence should be addressed to** Michael S. Levine, Ph.D. IDDRC, Semel Institute for Neuroscience, Room 58-258, UCLA School of Medicine, 760 Westwood Plaza, Los Angeles CA 90095, Tel: (310) 825-7595, Fax: (310) 206-5060, E-mail: mlevine@mednet.ucla.edu

**Cite as:** eNeuro 2015; 10.1523/ENEURO.0008-14.2015

**Alerts:** Sign up at eneuro.org/alerts to receive customized email alerts when the fully formatted version of this article is published.

Accepted manuscripts are peer-reviewed but have not been through the copyediting, formatting, or proofreading process.

This article is distributed under the terms of the Creative Commons Attribution License (http://creativecommons.org/licenses/by/3.0), which permits unrestricted use, distribution and reproduction in any medium provided that the original work is properly attributed.

Copyright © 2015 Society for Neuroscience

eNeuro Accepted Manuscript

eNeuro

http://eneuro.msubmit.net

eN-NWR-0008-14R2

# Enhanced GABAergic Inputs Contribute to Functional Alterations of Cholinergic Interneurons in the R6/2 Mouse Model of Huntington's Disease

This is a confidential document and must not be discussed with others, forwarded in any form, or posted on websites without the express written consent of eNeuro.

eNeuro Accepted Manuscript

# Enhanced GABAergic Inputs Contribute to Functional Alterations of Cholinergic Interneurons in the R6/2 Mouse Model of Huntington's Disease

Sandra M. Holley*, Prasad R. Joshi*, Anna Parievsky, Laurie Galvan, Jane Y. Chen, Yvette E. Fisher, My N. Huynh, Carlos Cepeda and Michael S. Levine
Intellectual and Developmental Disabilities Research Center, Semel Institute for Neuroscience and Human Behavior, University of California at Los Angeles, Los Angeles, CA 90095

* Denotes equal contribution.

**Abbreviated Title:** Striatal Cholinergic Interneurons in Huntington's Disease

**Author Contributions:** Designed research (MSL, CC), performed experiments and analyzed data (SMH, PRJ, AP, LG, JYC, YEF, MNH, CC, MSL), wrote the paper (SMH, PRJ, CC, MSL).

**Correspondence should be directed to:**
Michael S. Levine, Ph.D.
IDDRC, Semel Institute for Neuroscience, Room 58-258
UCLA School of Medicine
760 Westwood Plaza
Los Angeles CA 90095
Email: mlevine@mednet.ucla.edu
Tel: (310) 825-7595
Fax: (310) 206-5060

**No. of Figures:** 7
**No. of Tables:** 1
**Words in Abstract:** 250
**Introduction:** 508
**Discussion:** 1290

**Acknowledgments:** We thank Donna Crandall for help with illustrations.

**Conflict of Interest:** The authors have no conflicts of interest, financial or otherwise.

**Funding:** Funding was provided by CHDI, Inc. and USPHS NS41574.

eNeuro Accepted Manuscript

**Abstract**

In Huntington's disease (HD), a hereditary neurodegenerative disorder, striatal medium-sized spiny neurons undergo degenerative changes. In contrast, large cholinergic interneurons (LCIs) are relatively spared. However, their ability to release acetylcholine (ACh) is impaired. The present experiments examined morphological and electrophysiological properties of LCIs in the R6/2 mouse model of HD. R6/2 mice show a severe, rapidly progressing phenotype. Immunocytochemical analysis of choline acetyltransferase-positive striatal neurons showed that, although the total number of cells was not changed, somatic areas were significantly smaller in symptomatic R6/2 mice compared to wildtype (WT) littermates, For electrophysiology, brain slices were obtained from presymptomatic (3-4 weeks) and symptomatic (>8 weeks) R6/2 mice and their WT littermates. Striatal LCIs were identified by somatic size and spontaneous action potential firing in the cell-attached mode. Passive and active membrane properties of LCIs were similar in presymptomatic R6/2 and WT mice. In contrast, LCIs from symptomatic R6/2 animals displayed smaller membrane capacitance and higher input resistance, consistent with reduced somatic size. In addition, more LCIs from symptomatic mice displayed irregular firing patterns and bursts of action potentials. They also displayed a higher frequency of spontaneous GABAergic inhibitory postsynaptic currents (IPSCs) and larger amplitude of electrically evoked IPSCs. Selective optogenetic stimulation of somatostatin- but not parvalbumin-containing interneurons also evoked larger amplitude IPSCs in LCIs from R6/2 mice. In contrast, glutamatergic spontaneous or evoked postsynaptic currents were not affected. Morphological and electrophysiological alterations, in conjunction with the presence of mutant huntingtin in LCIs, could explain impaired ACh release in HD mouse models.

eNeuro Accepted Manuscript

**Significance Statement**

Although large cholinergic interneurons (LCIs) in striatum are spared in Huntington's disease (HD), deficits in cholinergic function have been described. Here we demonstrate in a mouse model of HD that the firing patterns of LCIs are disrupted and this is due to aberrant GABAergic neurotransmission. This explains cholinergic deficits in HD.

**Introduction**

Huntington's disease (HD) is a fatal, hereditary neurodegenerative disorder characterized by abnormal movements (chorea), cognitive impairment, and psychiatric disturbances (Bates et al., 2002). Histopathologically, there is progressive loss of cortical and striatal neurons with relative sparing of many (Ferrante et al., 1985; Ferrante et al., 1987; Reiner et al., 1988; Vonsattel and DiFiglia, 1998) but not all classes of striatal interneurons (Reiner et al., 2013). In the striatum, medium-sized spiny neurons (MSNs), the main projection neurons, undergo degenerative changes and, in animal models of HD, display a range of abnormal morphological and electrophysiological properties. These include decreased somatic areas (Levine et al., 1999) and loss of dendritic spines (Klapstein et al., 2001), as well as alterations in both passive and active membrane properties and synaptic activity (Klapstein et al., 2001; Cepeda et al., 2003; Cepeda et al., 2007).

Large cholinergic interneurons (LCIs) constitute a small percentage (~2%) of striatal neurons but they strongly modulate the functional status of MSNs in physiological and pathological conditions (Pisani et al., 2007; Ding et al., 2010). Excitatory glutamatergic inputs to LCIs are mainly provided by the thalamus and less so by the cerebral cortex (Lapper and Bolam, 1992; Sadikot et al., 1992; Smith and McCarron, 1998; Andre et al., 2008). MSNs and

eNeuro Accepted Manuscript

GABAergic interneurons provide inhibitory inputs to LCIs (Sullivan et al., 2008; Chuhma et al., 2011; Gonzales et al., 2013). Which properties or mechanisms endow LCIs with resistance to degeneration in HD remains unknown. One possibility is that LCIs receive only sparse cortical or thalamic inputs and N-methyl-D-asparate (NMDA) receptor-mediated responses are significantly smaller compared with those in MSNs (Cepeda et al., 2001). Indeed, cell swelling (an early sign of excitotoxicity) induced by prolonged application of NMDA produces a time-dependent increase in somatic area in MSNs whereas it produces negligible changes in LCIs (Cepeda et al., 2001). Another possibility is the fact that huntingtin nuclear inclusions form more gradually and are less abundant in LCIs compared with MSNs (Fusco et al., 1999; Kosinski et al., 1999; Meade et al., 2002).

Although spared in HD, LCIs display functional abnormalities including impaired ability to release ACh (Vetter et al., 2003; Smith et al., 2006; Farrar et al., 2011) and defective synaptic plasticity (Picconi et al., 2006). In order to elucidate the role of LCIs in the progression of HD symptoms, we examined morphological and electrophysiological changes in LCIs in the R6/2 genetic mouse model of HD. R6/2 mice with ~150 CAG (glutamine) repeats display a very aggressive form of the disease, more like juvenile HD (Mangiarini et al., 1996). They start to develop symptoms around 5-6 weeks of age and are fully symptomatic by 9-11 weeks. Using this model a progressive reduction of glutamatergic inputs onto MSNs was demonstrated (Cepeda et al., 2003), whereas GABAergic inputs were increased (Cepeda et al., 2004; Cepeda et al., 2013). Similar changes also have been observed in other genetic mouse models of HD (Cummings et al., 2010). In the present study, morphological, electrophysiological and optogenetic techniques were used to examine alterations of LCIs in the R6/2 model.

eNeuro Accepted Manuscript

## Material and Methods

### Animals

All experimental procedures were performed in accordance with the United States Public Health Service Guide for Care and Use of Laboratory Animals and were approved by the Institutional Animal Care and Use Committee at the University of California, Los Angeles (UCLA). Every effort was made to minimize pain and discomfort. R6/2 transgenic mice and wildtype (WT) littermates were obtained from the breeding colony in the institutional vivarium. These mice were maintained by crossing WT male C57BL/6xCBA mice with WT female C57BL/6xCBA mice that had transplanted R6/2 ovaries (both males and females purchased from The Jackson Laboratory). Genotyping was performed using PCR of DNA obtained from tail samples, once at weaning and again following use for experimentation to confirm the genotype. R6/2 mice (~150-160 repeat length) were utilized at pre-symptomatic (3-4 weeks) and symptomatic (>8 weeks) stages and compared with their WT littermates. For optogenetic experiments, somatostatin (SOM)-expressing interneurons and parvalbumin (PV)-expressing interneurons in WT and R6/2 mice were targeted by crossing homozygote male SOM-IRES-Cre mice ($Sst^{tm2.1(cre)Zjh}$/J) or male PV-IRES-Cre (B6.129P2-$Pvalb^{tm1(cre)Arbr}$/J) mice crossed with WT female C57BL/6xCBA mice transplanted with R6/2 ovaries (The Jackson Laboratory).

### ChAT immunostaining and cell counting

Experimenters blind to animal genotype performed these measurements. LCI somatic area measurements were obtained from symptomatic R6/2 mice and their WT littermates. Mice were perfused intracardially with 4% paraformaldehyde (PFA) in 0.1M phosphate buffered saline (PBS). Brains were then extracted and immersed in the same solution overnight. An antibody against choline acetyltransferase (ChAT) was utilized to visualize the LCIs in the striatum. Slices

eNeuro Accepted Manuscript

from WT and their R6/2 littermates were processed in tandem. Mouse brains were cryoprotected first in 20% sucrose/0.1M PBS solution then 30% sucrose/0.1M PBS solutions overnight and frozen with powdered dry ice. Coronal slices (30 µm) containing the striatum from each mouse were prepared using a Microm HM 505E cryostat and collected in wells containing 0.5 M Tris Buffered Saline (TBS, pH 7.4). Slices were then placed in a 10% methanol with 10% of 30% hydrogen peroxide TBS solution for 5 min to block endogenous peroxidases. After 3 washes (5 min each) in 0.05% Triton-TBS (pH7.4), slices were blocked in 1.5% normal rabbit serum (Vector S-5000) for 1 h and were then placed in goat anti-ChAT (Millipore, catalog number AB144P, 1:100) overnight at 4$^{o}$C. After another set of 3 washes (5 min each) in 0.05% Triton-TBS, slices were placed in rabbit anti-goat (Vector BA-5000, 1:300) for 35 min at room temperature. Slices were washed 3 times in 0.05% Triton-TBS for 5 min each and placed in Avidin Biotin Peroxidase Complex (Vector PK-6100) for 1 h followed by 3 more 5 min washes in 0.05% Triton-TBS. Slices were developed in diaminobenzadine, washed in cold TBS, mounted onto slides and coverslipped with Cytoseal XYL Mounting Media.

Stereological methods (Gundersen and Jensen, 1987) were used to determine striatal volume (excluding the nucleus accumbens). First, all slices containing the striatum [27 hemi-slices, thickness (H)=30 µm] were imaged using a 20x objective on a Zeiss microscope (Axio Imager.M2) and an AxioCam MR3 camera. All ChAT+ neurons were counted in each hemi-slice and 2 were randomly selected for somatic area measurements. Light homogeneity was ensured after adjusting the white balance and all images were acquired using the same light threshold. Measurements were obtained using the Zeiss AxioVision software (version 4.8.2 SP3). Volume estimates were obtained based on Cavalieri's principle using the following formula: Volume = d*(a1+a2+a3+a4 …), where d is the distance between serial sections (30 µm), and "a" is the area

eNeuro Accepted Manuscript

containing ChAT+ cells. ChAT+ cells as well as their diameters (h) were determined using the same software. For each slice, the ChAT+ cell number was corrected by the Abercrombie factor (N, where N=h/(h+H)). Then, the density (ChAT+ cells/$mm^3$) was obtained by dividing the corrected number of ChAT+ cells by the Cavalieri's striatal volume ($mm^3$).

**Electrophysiology in brain slices**

Mice were deeply anesthetized with halothane or isoflurane and decapitated. The brains were dissected and immediately placed in oxygenated ice-cold low-$Ca^{2+}$ artificial cerebrospinal fluid (ACSF) containing (in mM): 130 NaCl, 3 KCl, 1.25 $NaH_2PO_4$, 26 $NaHCO_3$, 5 $MgCl_2$, 1 $CaCl_2$, and 10 glucose. Coronal slices (300 μm) were cut and transferred to an incubating chamber containing ACSF (with 2 mm $CaCl_2$ and 2 mm $MgCl_2$) oxygenated with 95% $O_2$-5% $CO_2$ (pH 7.2-7.4, osmolality 290-310 mOsm, 25±2°C). A single slice was then transferred to a submerged recording chamber fixed to an upright microscope. LCIs were visualized in the dorsolateral striatum using infrared illumination with differential interference contrast optics (IR-DIC microscopy) and identified based on large somatic size (at least twice the size of a typical MSN), basic membrane properties, as well as their characteristic tonic action potential firing observed in the cell-attached mode.

The patch pipette (series resistance 3-5 MΩ) contained the following solution (in mM): 130 Cs-Methanesulfonate, 10 CsCl, 4 NaCl, 1 $MgCl_2$, 5 MgATP, 5 EGTA, 10 HEPES, 0.5 GTP, 10 phosphocreatine, 0.1 leupeptin (pH 7.25–7.3, osmolality, 280–290 mOsm) (Cs-Meth solution). In a subset of experiments, CsCl-based internal solution with a higher concentration of $Cl^-$ ions (140 mM) was used (CsCl solution). Access resistances were <20 MΩ and all the recordings were made at ambient temperature (22-26º C).

eNeuro Accepted Manuscript

To examine firing patterns and pacemaking of LCIs 2-5 min periods of spontaneous activity in the cell-attached configuration were analyzed. The Mini Analysis program (Justin Lee, Synaptosoft) was used to calculate inter-spike intervals (ISI) from which the degree of autocorrelation and coefficient of variation can be derived. Degree of autocorrelation was defined as a function of the coefficient value (peak amplitude of the first lag period) and the number of peaks away from lag 0. Autocorrelations were assigned high or low ratings based on correlation coefficients and visual inspection of the histograms from each cell. A histogram with high autocorrelation had correlation coefficients >0.2 (first peak value range 0.203–0.8) and showed additional peaks at different lag periods, while a low autocorrelation had correlation coefficients <0.2 (first peak value range 0.08–0.2) and showed only 1–2 peaks. Cells with no correlation showed no peaks except at the origin (lag 0) where the correlation is always 1 (this peak was eliminated from the autocorrelograms). This criterion to define cells with high or low degree of autocorrelation was used in a previous publication (Cepeda et al., 2014). The coefficient of variation, a common measure of dispersion of a probability distribution, was defined as the ratio of the standard deviation (SD) to the calculated mean ISI (Bennett and Wilson, 1999). LCIs with high coefficient of variation had low degree of autocorrelation and *vice versa*.

Spontaneous postsynaptic currents were recorded in the whole-cell configuration in standard ACSF and in the presence of appropriate receptor blockers. Membrane current was filtered at 1 kHz and digitized at 200 μs using Clampex 8.2 (gap-free mode). Cells were voltage-clamped at -70 mV to determine basic membrane properties using a depolarizing voltage command (10 mV). Glutamate receptor mediated spontaneous excitatory postsynaptic currents (sEPSCs) were recorded in the presence of the $GABA_A$ receptor blocker, bicuculline (BIC, 10

eNeuro Accepted Manuscript

μM). As the frequency of spontaneous EPSCs is generally very low in LCIs, in another set of experiments 4-Aminopyridine (4-AP, a selective $K^+$-channel blocker) was co-applied (100 μM) to enhance neurotransmitter release and increase the frequency and amplitude of sEPSCs. Application of the α-amino-3-hydroxy-5-methyl-4-isoxazolepropionic acid (AMPA) receptor blocker, 2,3-dihydroxy-6-nitro-7-sulfamoyl-benzo[f]quinoxaline-2,3-dione (NBQX, 10 μM) and the N-methyl-D-aspartate (NMDA) receptor blocker amino-5-phosphonovaleric acid (APV, 50 μM) abolished all spontaneous EPSC activity (data not shown). Evoked glutamatergic EPSCs (eEPSCs) were recorded at -70mV. Lidocaine (QX314, 4 mM) was added to the internal pipette solution to block $Na^+$ channel-mediated currents. To evoke synaptic currents in LCIs, a monopolar glass stimulating-electrode (patch-pipette filled with ACSF) was placed in the striatum approximately 150-200 μm dorsal to the recorded cell. Test stimuli (0.5 ms duration) were applied every 20 s and responses averaged over two to three consecutive trials. Test stimuli were applied at increasing stimulus intensities (0.01–0.10 mA) to assess input–output functions. These recordings were obtained in the presence of BIC (10 μM). Co-application of NBQX (10μM) and APV (50μM) completely blocked the evoked currents.

To assess $GABA_A$ receptor mediated spontaneous synaptic activity, cells were voltage clamped at +20mV and spontaneous inhibitory postsynaptic currents (sIPSCs) were recorded in the presence of ionotropic glutamate receptor blockers (10 μM NBQX and 50 μM APV). Alternatively, sIPSCs also were recorded with cells voltage clamped at -70 mV with the pipette solution containing a high concentration (140 mM) of $Cl^-$ ions. Tetrodotoxin (TTX, 1 μM) was added to record miniature (m) IPSCs. Evoked IPSCs (eIPSCs) were recorded at +10 mV, using the Cs-Meth internal solution or at -70 mV using the high $Cl^-$ solution. QX314 was added to the patch pipette solution to block $Na^+$ channel-mediated currents. These recordings were obtained

eNeuro Accepted Manuscript

in the presence of ionotropic glutamate receptor blockers as indicated above. In both sets of experiments, BIC (10 μM) blocked spontaneous or eIPSCs (data not shown). Spontaneous EPSCs and IPSCs were analyzed offline using the Mini Analysis Program. Evoked synaptic currents were analyzed using pClamp 8.2 or 10.2 (Molecular Devices).

**AAV stereotaxic injections and optical stimulation**

Stereotaxic injections of Channelrhodopsin-2 (ChR2) in SOM-Cre and PV-Cre mice crossed with R6/2 or WTs were performed at 4-5 weeks of age. Mice were anesthetized with isoflurane and injected with an adeno-associated virus (AAV2) expressing DIO-channelrhodopsin-2 (ChR2(H134R)) and enhanced yellow fluorescent protein (EYFP). This construct contained a floxed stop codon and the EF1a promoter was used for protein expression (Cardin et al., 2009; Sohal et al., 2009). One microliter of virus (titer: $9.45x10^{12}$ vg/ml) was injected into each striatum at a rate of 0.2 μl/min and at the following stereotaxic coordinates from bregma: AP 1.0 mm, ML +/-2.0 mm and DV -3.3 mm from the dura. For the thalamus in R6/2 and WT mice, an AAV2 construct with ChR2(H134R)-EYFP under the $Ca^{2+}$/calmodulin-dependent protein kinase type II alpha subunit (CaMKIIa) promoter (titer: $1.14x10^{13}$ vg/ml) was injected. Bilateral injections (0.25 μl) were made in the centre median-parafascicular (Cm/Pf) intralaminar nuclear complex of the thalamus (AP -2.2 mm, ML +/- 0.7 mm, DV -3.5 mm) at a rate of 0.1 μl/min. All ChR2 plasmids were obtained from Karl Deisseroth (Stanford University) and AAV production was performed at the University of Iowa Gene Transfer Vector Core.

In order to ensure sufficient expression of injected AAVs, recordings were performed at least 5-9 weeks following injections. PV- and SOM-expressing interneurons were activated with a single light pulse (470 nm, 0.5 ms, 10 mW, CoolLED) delivered through the epifluorescence illumination pathway using Chroma Technologies filter cubes. eIPSCs were recorded in LCIs in

eNeuro Accepted Manuscript

voltage clamp mode, with a Cs-Meth based internal solution at a holding potential of +10 mV and in the presence of glutamatergic receptor antagonists. In these experiments, biocytin (0.2 %) was also included in the patch pipette to locate recorded LCIs.

For thalamic stimulation, excitatory responses were evoked by a brief light pulse (470 nm, 1 ms duration, 5 mW) in the presence of 10 µM BIC. AMPA currents were recorded in LCIs at a holding potential of -70mV. NMDA currents were recorded at a holding potential of +40mV in the presence of BIC and NBQX (10 µM). Patch pipettes were filled with Cs-Meth solution containing 4 mM QX-314 and 0.2% biocytin. To prevent stimulation of thalamocortical inputs, the cerebral cortex was removed from the slice before recording.

**Electrophysiology in acutely isolated neurons**

Some slices also were used to record from acutely isolated large (presumably cholinergic) neurons. With the aid of a dissecting microscope, the dorsal striatum was dissected and incubated for at least 1 h at room temperature in an $NaHCO_3$-buffered Earle's balanced salts solution (Sigma-Aldrich) supplemented with (in mM): 1 pyruvic acid, 0.005 glutathione, 0.1 NG-nitro-L-arginine and 1 kynurenic acid (pH 7.4; aerated with 95% $O_2$/5% $CO_2$; 300-310 mOsm/l). After incubation, a slice was placed in an oxygenated cell-stir chamber (Wheaton, Millville, NJ) and enzymatically treated for 20 min with papain (0.5 mg/ml; Calbiochem) at 35ºC in a N-[2-hydroxyethyle] piperazine-N-[2-ethanesulfonic acid) (HEPES)-buffered Hank's balanced salts solution (Sigma Aldrich) and supplemented as described above. After enzymatic digestion, the tissue was rinsed with low-$Ca^{2+}$ HEPES-buffered $Na^+$ isethionate solution containing (in mM): 140 $Na^+$ isethionate, 2 KCl, 2 $MgCl_2$, 0.1 $CaCl_2$, 23 glucose and 15 HEPES (pH 7.4, 300-310 mOsm/l). Striatal slices were then mechanically dissociated with a series of graded fire-polished Pasteur pipettes. The cell suspension was then plated into a 35 mm Nunclon Petri dish containing

eNeuro Accepted Manuscript

a HEPES-buffered salt solution (in mM: 140 NaCl, 23 glucose, 15 HEPES, 2 KCl, 2 $MgCl_2$ and 1 $CaCl_2$; pH 7.4, 300-310 mOsm/l) and mounted on the stage of an upright fixed-stage microscope (Zeiss Axioscope, Thornwood, NY).

The whole-cell patch clamp technique in voltage clamp mode was used for recordings. Large neurons were identified based on somatic size (at least twice the size compared to MSNs). Signals were detected with an Axoclamp 2B amplifier (Axon Instruments). Glass pipettes (2.5-3.5 MΩ) were filled with an internal solution consisting of (in mM) 175 N-methyl-D-glucamine, 40 HEPES, 2 $MgCl_2$, 10 ethylene glycol-bis (β-aminoethyl ether)-N,N,N',N'-tetraacetic acid (EGTA), 12 phosphocreatine, 2 $Na_2ATP$, 0.2 $Na_2GTP$ and 0.1 leupeptin (pH 7.25, 265-270 mOsm/l). The $Mg^{2+}$-free external solution consisted of the following (in mM): 135 NaCl, 20 CsCl, 3 $BaCl_2$, 2 $CaCl_2$, 10 glucose, 10 HEPES, 0.02 glycine and 0.0003 TTX (pH 7.4, 300-310 mOsm/l). After obtaining a GΩ seal and rupturing the membrane to create the whole-cell configuration, access resistances were <20 MΩ. Series resistance was then compensated (70-90%) and monitored throughout the experiment.

Drugs were applied through an array of capillaries positioned 500-600 µm from the cell, using a pressure-driven fast perfusion system. Solution changes were performed by changing the position of the array with a DC drive system controlled by a SF-77B perfusion system (Warner Instruments). Drugs were applied for 3 s every 30 s. Values for peak currents and current densities were calculated for all neurons. Current densities were calculated by dividing the peak current by the cell capacitance and currents were normalized to cell size.

**Statistics**

Differences between group means were assessed with appropriate t-tests (paired or unpaired) or Mann-Whitney Rank Sum test, Chi-square or Fisher Exact tests for proportions, and

eNeuro Accepted Manuscript

299 appropriately designed analyses of variance (two-way ANOVA with or without repeated
300 measures, followed by Bonferroni's or Tukey's post-hoc tests). Values in figures and text are
301 presented as mean±standard error of the mean (SEM). Differences were considered statistically
302 significant if $p<0.05$. In all figures and in Table 1, * indicates $p<0.05$,** indicates $p<0.01$ and
303 *** indicates $p<0.001$.
304
305 **Results**
306 **LCI somatic areas are reduced in R6/2 mice**
307 Reduced MSN somatic area and dendritic elaboration have been previously shown in
308 symptomatic R6/2 mice (Levine et al., 1999; Klapstein et al., 2001). However, morphological
309 changes in LCIs have not been examined. We used ChAT immunohistochemistry to estimate cell
310 numbers and changes in somatic area of LCIs in symptomatic R6/2 mice (n=4, age 64±2 days)
311 and WT littermates (n=4, age 60±2 days). LCIs (n=202 cells) from R6/2 mice showed a
312 statistically significant decrease in somatic area compared to LCIs (n=202 cells) from WT mice
313 ($p<0.01$) (Fig. 1A, B). To estimate changes in ChAT+ neuronal density, the area of individual
314 slices was calculated first. Compared with WT littermates, mean striatal area of 30 µm thick
315 hemi-slices was significantly smaller in R6/2 compared to WT mice ($p=0.011$). Stereological
316 methods were used to calculate striatal volume and LCI total number and density. Striatal
317 volume was significantly reduced in R6/2 compared to WT mice ($p=0.029$) but the total numbers
318 of ChAT+ neurons were not significantly different ($p=0.33$). However, the stereological analysis
319 revealed a statistically significant increase in striatal ChAT+ neuronal density ($p=0.013$) (Fig.
320 1B).
321 **Passive and active membrane properties of LCIs are altered in HD mice**

eNeuro Accepted Manuscript

For electrophysiological studies LCIs were recorded primarily from the dorsolateral striatum. Representative IR-DIC images of visually identified LCIs from WT and R6/2 mice are shown in Fig. 2A. In whole-cell voltage clamp mode, passive membrane properties were consistent with LCIs, displaying relatively high input resistance and fast decay time constant. No differences in membrane properties of LCIs from WT and presymptomatic R6/2 animals (n=4 in each group, age 23±1 days) were observed (Table I). In symptomatic animals (n=10, age 65±1 days) LCIs displayed significantly lower mean capacitance ($p=0.038$) and higher mean input resistance ($p<0.001$) compared with WT animals (n=14, age 65±1 days).

Most LCIs from WT and R6/2 mice generated spontaneous action potentials in the cell-attached configuration at frequencies ranging between 0.3-3.9 Hz. To calculate the mean firing frequency, cell-attached recordings were obtained over a 2-5 min period. No differences were seen in LCI firing rates from presymptomatic R6/2 mice and WT littermates (data not shown). Mean firing frequencies (Fig. 2H) also were similar in LCIs from symptomatic R6/2 mice (Fig. 2C) compared with WTs (Fig. 2B). However, more LCIs from R6/2 mice displayed irregular firing patterns and bursts (Fig. 2D). Autocorrelation analysis of LCI firing demonstrated that about twice as many cells from WTs (10/33, 30.3%) displayed high degree of autocorrelation compared with LCIs from R6/2s (5/39, 12.8%). To obtain a quantitative estimate of firing regularity, in a subset of cells (those that displayed some degree of autocorrelation, n=20 WT and n=26 R6/2) the coefficient value of the first lag period (adjacent to lag 0) was calculated using autocorrelation histograms (Fig. 2E-G). The average values were significantly higher in cells from WT compared to cells from R6/2 mice (0.29±0.04 and 0.21±0.02 respectively) ($p=0.046$) (Fig. 2I), suggestive of decreased firing regularity in LCIs from R6/2 mice.

eNeuro Accepted Manuscript

Another way to examine firing regularity is to compute coefficients of variation, the lower the coefficient the higher the regularity. Using 0.2 as the cutoff value to match the average autocorrelation coefficients, more cells from WTs (11/33, 33.3%) had low coefficients of variation (<0.2) compared with those from R6/2s (4/39, 10.2%). The difference between groups was statistically significant (p=0.02). Finally, scatter plots demonstrated a strong correlation between coefficients of variation and firing frequency in LCIs from WT mice (linear regression, $r^2$=0.52, p<0.001), whereas in cells from R6/2 mice this correlation was greatly reduced ($r^2$=0.06, p=0.14) (Fig. 2J). Similarly, the Pearson Product Moment correlation demonstrated a very high correlation in LCIs from WTs (-0.72, p<0.0001) whereas the correlation was not statistically significant in cells from R6/2 mice (-0.24, p=0.14). Together, these data provide evidence that the ability of LCIs to regularly generate action potentials becomes compromised in symptomatic mice, suggesting alterations in intrinsic conductances and/or synaptic inputs.

**Spontaneous $GABA_A$ receptor-mediated synaptic currents are increased in LCIs from symptomatic R6/2 mice.**

MSNs from symptomatic R6/2 mice receive increased GABAergic inputs and feedforward inhibitory circuits play a major role in this effect (Cepeda et al., 2013). To determine if LCIs also are subject to increased GABAergic inhibition, sIPSCs were recorded (in the presence of ionotropic glutamate receptor antagonists) using the Cs-Meth internal solution and cells were held at +20 mV to increase the driving force of $Cl^-$ ions. The frequency of sIPSCs (1.7±0.3 Hz in WT versus 1.1±0.6 Hz in R6/2, p=0.42) was not significantly different in LCIs from presymptomatic R6/2 compared to WT mice (n=4 in each group, age 23±1 days). In contrast, in symptomatic R6/2 mice (n=10, age 64±1 days) the average frequency of sIPSCs was significantly increased compared with WTs (n=12, age 65±1 days) (Fig. 3A, C right inset). This

eNeuro Accepted Manuscript

increase was observed across amplitude bins and was statistically significant for the 10-20 pA bin (Fig. 3C). Further, the cumulative inter-event interval probability distribution was shifted to the left, indicating more short inter-event intervals in cells from R6/2 mice ($p<0.001$) (Fig. 3E). Application of TTX (1 μM) eliminated the increase in sIPSC frequency (Fig. 3D1), indicating its dependence on presynaptic action potentials. In addition, the percent reduction in IPSC frequency after TTX application was greater in cells from R6/2 compared with WT mice, suggesting that more sIPSCs from R6/2 cells were action potential-dependent (Fig. 3G, second bar graph).

We also examined the frequency of GABAergic sIPSCs in WT (n=12, age 65±1 days) and symptomatic R6/2 animals (n=13, age 64±2 days) using a CsCl-based internal solution with the cell voltage-clamped at -70 mV and in the presence of glutamate receptor blockers. Mean sIPSC frequency was significantly greater in LCIs from R6/2 mice ($p<0.01$) (Fig. 3B, D right inset). The amplitude-frequency histogram showed that, except for the 10-20 pA bin, increased frequency occurred across all other amplitude bins (Fig. 3D), in particular IPSCs with amplitudes between 20-40 pA ($p<0.001$). The cumulative inter-event interval probability distribution also was significantly shifted to the left in LCIs from R6/2 mice ($p<0.001$) (Fig. 3F). Similar to results obtained with Cs-Meth solution, the frequency of mIPSCs in LCIs recorded with CsCl after TTX were not significantly different between WTs and R6/2s (Fig. 3H). The percent change in frequency after TTX was significantly reduced in LCIs from R6/2s ($p=0.02$) (Fig. 3H right bar graph), indicating that more sIPSCs were dependent on presynaptic action potentials.

**Evoked GABAergic currents are increased in LCIs from symptomatic R6/2 mice**

eIPSCs were recorded at +10mV in the presence of glutamate receptor antagonists. Intrastriatal stimulation typically evoked polysynaptic GABAergic currents with two or more peaks (Fig. 4A,

eNeuro Accepted Manuscript

C). Application of BIC (10 μM) completely blocked all evoked currents. Amplitude of peak current with the shortest latency, presumably monosynaptic, was measured (arrows in Fig. 4A, C). eIPSC peak currents were similar over a range of stimulus intensities (0.01-0.06 mA) in LCIs from WT and presymptomatic R6/2 mice (data not shown). In LCIs from symptomatic animals (n=3, age 61±3 days), mean peak currents recorded at +10 mV holding potential using the Cs-Meth internal solution were significantly larger ($p<0.001$) than in LCIs from WT mice (n=3, age 66±5 days) (Fig. 4B). Evoked GABAergic currents also were examined using high $Cl^-$ internal solution, with cells voltage-clamped at -70 mV. Under these conditions, intrastriatal stimulation also typically evoked polysynaptic inward currents with characteristic multiple peaks (Fig. 4C). Amplitudes of peak currents with the shortest latency were significantly greater across a range of stimulus intensities in LCIs from R6/2 compared with mice ($p<0.001$) (Fig. 4D).

To determine the possible source of increased GABA responses at the pre- or post-synaptic sites, paired-pulse ratios (PPRs) were calculated for eIPSCs at different interpulse intervals (25, 50 and 100 ms). The differences in PPRs were not statistically significant in LCIs from R6/2 mice (at 25 ms interval, 1.22±0.4 and 1.07±0.3; at 50 ms interval, 1.26±0.8 and 1.18±0.7; at 100 ms interval, 1.01±0.5 and 0.85±0.4 in WT and R6/2, respectively).

**LCI responses to optogenetic activation of SOM- but not PV-expressing interneurons are increased in HD compared to WT mice**

Feedforward inhibition, in particular from SOM-expressing persistent low-threshold spiking (PLTS) interneurons, plays a crucial role in the increased GABA synaptic activity observed in MSNs from R6/2 mice (Cepeda et al., 2013). To determine if SOM-expressing PLTS interneurons serve as a source for increased GABA synaptic activity in LCIs, we used an optogenetic approach to isolate the contribution of these interneurons (Fig. 5A). LCIs were

eNeuro Accepted Manuscript

voltage clamped at +10 mV and IPSCs were evoked by optically activating ChR2 expressed in SOM interneurons (Fig. 5B, upper traces). In LCIs from WT mice (n=7, age 71±2 days) 62% of cells responded to SOM interneuron activation (8/13) and in LCIs from R6/2 mice (n=6, age 70±1 days) 82% of cells responded (9/11 cells) ($p=0.27$). The eIPSCs in LCIs from R6/2 mice had significantly larger peak amplitudes ($p<0.05$), greater charge ($p<0.05$ pA) (Fig. 5C) and longer decay times (125±8 ms versus 98±10 ms, $p<0.05$ for R6/2 and WT, respectively) when compared to responses recorded in WT LCIs. All eIPSCs were identified as GABAergic as all recordings were performed in the presence of NBQX and APV (10 µM and 50 µM, respectively), and responses were completely eliminated after addition of BIC (10 µM) (Fig. 5B, lower traces).

We also examined the effects of optical activation of PV-expressing, fast-spiking interneurons (FSIs) in symptomatic R6/2 (n=6, age 74±1 days) and WT littermates (n=7, age 78±3 days). PV interneuron activation produced few IPSC responses in LCIs from R6/2 (10/16, 59%) and WT (8/21, 38%) mice ($p=0.19$) and the amplitude of the response was much smaller compared with responses evoked by SOM-expressing interneurons (Fig. 5D, E). When comparing the evoked responses, there was no difference in the peak amplitude, charge (Fig. 5F), or decay times (R6/2 74±16 ms versus WT 86±26 ms) in LCIs from R6/2 compared to WT. These results suggest that SOM-positive PLTS interneurons, and not PV-positive FSIs, contribute to the increased GABAergic inputs to LCIs of symptomatic R6/2 mice. Although it could be argued that the small and inconsistent GABA responses evoked by PV terminals in LCIs could be explained by insufficient expression of ChR2, this is unlikely as previous studies using similar Cre lines demonstrated large responses to PV activation in MSNs (Cepeda et al.,

eNeuro Accepted Manuscript

435 2013). This was corroborated in the present study by recording consistent, large-amplitude
436 GABA responses in a small number of MSNs adjacent to LCIs (not shown).
437
438 **Spontaneous and evoked glutamatergic currents**
439 Excitatory synaptic inputs also could alter tonic firing patterns of LCIs. Spontaneous
440 glutamatergic EPSCs were measured in LCIs, with cells voltage-clamped at -70mV, in the
441 presence of BIC (10 μM). Consistent with previous studies (Bennett and Wilson, 1999) very few
442 sEPSCs were observed under these conditions. Subsequently, the frequency of sEPSCs was
443 enhanced by co-application of 4-AP (100 μM), a $K^+$ channel blocker that enhances
444 neurotransmitter release. Average sEPSC frequencies (7.8±3.4 Hz, n=6 WT and 4.4±1.4 Hz, n=6
445 R6/2, p=0.3), amplitude-frequency histograms and cumulative probability of inter-event intervals
446 were not significantly different in LCIs from R6/2 mice (n=4, age 76±6 days) and their WT
447 littermates (n=4, age 74±6 days) (not shown).
448 eEPSCs were recorded at -70 mV with QX314 in the internal pipette solution (Fig. 6A).
449 Similar procedures to those described above were used to evoke synaptic currents in LCIs.
450 Application of NBQX (10 μM) and APV (50 μM) completely blocked evoked currents. There
451 were no statistically significant differences in peak amplitudes of LCIs from symptomatic R6/2
452 (n=8, age 65±1 days) compared with those from WTs (n=6, age 66±2 days) at all stimulation
453 intensities (Fig. 6A, B).
454 **LCI responses to optogenetic activation of thalamic inputs are similar in WT and R6/2**
455 **mice.**
456 The main excitatory input onto LCIs has been shown to emanate from the thalamus (Lapper and
457 Bolam, 1992). Expression of ChR2 in the Cm/Pf nuclear complex allows stimulation of specific

eNeuro Accepted Manuscript

thalamostriatal projections onto LCIs. These projections are glutamatergic and when stimulated, result in eEPSCs. At a holding potential of -70 mV, in the presence of BIC, the eEPSC is attributable to activation of AMPA receptors (Fig. 6D, upper traces). Amplitude and charge of AMPA currents in R6/2 mice (n=12, age 75±2 days) were similar to those from WTs (n=13, age 79±2 days) (Fig. 6D, E). Decay times also were similar (37±7 ms in WT and 23±4 ms in R6/2). At a holding potential of +40 mV, in the presence of BIC and NBQX, the eEPSC is attributed to currents through activation of NMDA receptors (Fig. 6D, lower traces). NMDA currents showed no differences in peak amplitude, charge, or kinetics between WT and R6/2 mice (Fig. 6E).

**Glutamate and GABA responses in acutely dissociated LCIs are similar in WT and R6/2 mice**

To more directly evaluate postsynaptic mechanisms, $GABA_A$ receptor-mediated currents were examined in the acutely isolated LCIs in R6/2 mice (n=5, age 71±4 days) and WT littermates (n=6, age 69±3 days). Large cells, presumably LCIs, were identified based on somatic size as well as thick proximal dendritic processes. A range of concentrations (10, 100, 1000 μM) was used to examine the effects of GABA application. GABA-induced peak current densities were not significantly different in LCIs from R6/2 compared to WT mice (Fig. 7A, B).

AMPA and NMDA mediated currents also were assessed in the acutely isolated striatal neuronal preparation, using $Mg^{2+}$-free recording solution. AMPA-induced peak current densities were similar in large cells from WT and R6/2 mice (Fig. 7C). NMDA-induced peak current densities also were similar in large cells from WT and R6/2 mice at a range of concentrations (Fig. 7D).

**Discussion**

eNeuro Accepted Manuscript

The present findings indicate that both morphological and electrophysiological alterations occur in LCIs from symptomatic R6/2 mice. These changes occur in parallel to the reduced capacity for ACh synthesis/release (Vetter et al., 2003; Smith et al., 2006; Farrar et al., 2011). Morphologically, somatic areas of LCIs were smaller than those of WT littermates. In agreement, the cell membrane capacitance was significantly decreased while the input resistance was significantly increased in LCIs from R6/2 mice. Although the mean spontaneous firing frequency of LCIs was not altered in R6/2 mice, the firing patterns were significantly affected. More LCIs from R6/2 mice displayed irregular firing and bursts compared to WT littermates, suggesting that the regular, tonic firing ability of LCIs is disrupted in HD. One possible reason firing patterns are altered is that, similar to MSNs, striatal LCIs from symptomatic R6/2 mice show increased GABAergic synaptic inhibition. Optogenetic studies indicated that a likely source of increased inhibition is the SOM- but not the PV-expressing interneurons. Altered firing patterns, in conjunction with increased GABA inhibition and reduced somatic size, could partially explain decreased production and release of ACh in HD.

Striatal ACh plays a pivotal role in attention and cognitive processes (Graybiel, 1990, 1995; Ding et al., 2010). ACh synthesis and release are significantly altered in a number of neurological diseases (Bird, 1980; Pisani et al., 2007). For example, Parkinson's disease and dystonia have been classically considered as hypercholinergic disorders (Pisani et al., 2007). In agreement, ablation of LCIs attenuates L-DOPA induced dyskinesia in mice rendered parkinsonian (Won et al., 2014). In contrast, in HD decreased production and release of ACh occur (Vetter et al., 2003; Smith et al., 2006; Farrar et al., 2011), which would contribute to behavioral and cognitive deficits. Furthermore, in animal models of HD, LCIs fail to express LTP which is a requirement for depotentiation of MSNs and behavioral flexibility (Picconi et al.,

eNeuro Accepted Manuscript

504 2006). The cause for decreased expression of ACh markers in HD remains unknown. However,
505 the findings presented here provide evidence for potential mechanisms.

506 While the average firing frequency of LCIs was not different in R6/2 and WT animals,
507 the firing pattern was altered. Specifically, regular firing was less prominent in LCIs from HD
508 mice. In slice studies, different types of LCI firing have been observed including regular,
509 irregular and bursting (Bennett and Wilson, 1999). In the present study similar LCI firing
510 patterns were found, but the proportions were different with more LCIs from R6/2 mice firing
511 irregularly and in bursts. While spontaneous tonic firing of LCIs has been shown to depend on a
512 combination of $Na^+$ and $I_h$ currents, the transition to burst firing depends on small conductance
513 $Ca^{2+}$-activated $K^+$ (SK) channels (Bennett et al., 2000). In HD mouse models, a number of $K^+$
514 conductances are deficient (Ariano et al., 2005; Tong et al., 2014). It is thus possible that $I_h$
515 and/or SK channels also are altered in HD animals, which could explain more irregular firing and
516 bursting compared to WT animals.

517 Although tonic firing of LCIs largely depends on intrinsic conductances (Bennett and
518 Wilson, 1999; Bennett et al., 2000), synaptic inputs can also modulate LCI firing (Bennett and
519 Wilson, 1998). In fact, one critical issue in trying to determine the cause of altered ACh release
520 in HD is whether or not excitatory and inhibitory inputs onto LCIs are affected (Farrar et al.,
521 2011). Anatomical studies have shown that LCIs receive GABA inputs from both direct and
522 indirect pathway MSNs, as well as from GABAergic interneurons (Gonzales et al., 2013). Here,
523 similar to MSNs (Cepeda et al., 2013), LCIs from symptomatic R6/2 mice received increased
524 GABAergic inputs, which would disrupt regular firing and ACh release. While the exact
525 source(s) of increased GABAergic inputs remains unknown, it is likely that feedforward
526 inhibition has an important role. The fact that in the presence of TTX the increase in GABAergic

eNeuro Accepted Manuscript

activity no longer occurred, along with similar GABA responses in WT and R6/2 dissociated LCIs, indicates an action potential-dependent presynaptic mechanism. As in the present recording conditions only PLTS interneurons fire spontaneously, it is likely that these interneurons contribute to increased GABA activity. In support, optogenetic stimulation of SOM-expressing GABA interneurons, but not that of PV-expressing interneurons, produced larger responses in LCIs from R6/2 mice. The cause of increased excitability of PLTS interneurons in HD is uncertain. This class of interneurons is resistant to degeneration and ubiquitinated intranuclear inclusions occur very rarely (Kosinski et al., 1999). However, it has been shown that PLTS interneurons fire at higher rates in HD mouse models and are less subject to inhibitory inputs (Cepeda et al., 2013).

The present findings are in general agreement with anatomical data showing that about 60% of all synaptic inputs to LCIs are GABAergic (Gonzales et al., 2013). About 24% of this innervation is from MSN axon collaterals and only 10% is from striatal and/or pallidal PV-expressing neurons. Indeed, similar to our data, while optogenetic stimulation of PV-expressing interneurons induced reliable GABA synaptic responses in MSNs, such stimulation produced no responses in neighboring LCIs (Szydlowski et al., 2013). This means that the bulk of GABA inputs to LCIs come from SOM- or NPY-expressing interneurons. Although a small contribution of MSN input to LCIs cannot be completely ruled out, this possibility is unlikely as MSNs recorded *in vitro* are usually very hyperpolarized and do not fire spontaneous action potentials, even though they are more depolarized in symptomatic animals. Additional studies using D1- and D2-Cre animals could sort this out. Interestingly, there is anatomical evidence that the LCI input from direct pathway MSNs is more prevalent than that from indirect pathway MSNs (Martone et al., 1992).

eNeuro Accepted Manuscript

Excitatory synaptic inputs also could affect LCI firing rates. Most glutamatergic inputs come from thalamic nuclei (Lapper and Bolam, 1992), are very sparse (representing only about 13% of all synapses) and are localized to the more distal dendrites (Gonzales et al., 2013). Very low spontaneous glutamatergic synaptic activity onto LCIs was found and it was similar in cells from WT and HD animals. In order to increase glutamate release 4-AP was bath applied. No significant difference in average frequency of sEPSCs occurred in the presence of 4-AP indicating that excitatory inputs, at least *in vitro*, are not a likely source of variation in LCI firing, Consistent with this observation, EPSCs evoked by electrical stimulation within the striatum or by specific optogenetic activation of thalamic inputs produced similar responses in LCIs from WT and R6/2 mice. In addition, postsynaptic responses evoked by glutamate receptor agonists in dissociated LCIs were not different.

Together these data demonstrate that, although in HD there is no loss of LCIs, morphological and electrophysiological abnormalities occur in symptomatic R6/2 mice. However, how changes in firing patterns translate into decreased cholinergic markers in these mice remains an open question. We can only speculate that in order to maintain adequate ACh levels tonic, pacemaker firing of LCIs is required. Phasic bursting and long pauses may disrupt ACh levels and release. In addition, reduced somatic area and possible axonal branching loss could also contribute to reduced ACh markers. Finally, the presence of mutant huntingtin in LCIs could also affect synthesis, transport and/or release of ACh in spite of no changes in firing rate.

Disruption of regular firing of LCIs can have profound implications in HD. Studies have shown that ACh, acting on muscarinic receptors in corticostriatal terminals, can regulate excitatory input onto MSNs (Pakhotin and Bracci, 2007; Ding et al., 2010). Dysregulated glutamate release is a key feature in the early stages of HD (Cepeda et al., 2007) and it is likely

eNeuro Accepted Manuscript

573 that altered ACh transmission plays a role. Finding ways to restore normal firing patterns of LCIs
574 and prevent altered glutamate inputs could help in the treatment of behavioral and cognitive
575 deficits in HD.

eNeuro Accepted Manuscript

**Table I**

**Passive Membrane Properties of LCIs in R6/2 Mice**

| | Cm (pF) | Rm (MΩ) | Tau (ms) |
|---|---|---|---|
| **Pre-symptomatic** | | | |
| WT (n=10) | 89.5±7 | 151±22 | 1.2±0.2 |
| R6/2 (n=12) | 81.4±5 | 177±28 | 0.9±0.1 |
| **Symptomatic** | | | |
| WT (n=31) | 89.6±4 | 198±15 | 1.3±0.1 |
| R6/2 (n=26) | 80.0±3* | 335±23*** | 1.2±0.1 |

eNeuro Accepted Manuscript

585 **Figure legends**

586 **Figure 1**

587 **A.** LCIs were stained with ChAT antibody in WT and symptomatic R6/2 mice. Less intense
588 staining and reduced cell size were evident**. B.** Bar graphs show that the mean somatic cross-
589 sectional area was significantly smaller in R6/2 LCIs. In addition, mean striatal area was
590 significantly reduced in hemi-slices from R6/2 mice. Striatal volume assessed stereologically
591 also was significantly reduced. The number of striatal ChAT+ neurons was similar but, because
592 of reduced striatal volume, the mean density of ChAT+ neurons was significantly increased in
593 R6/2 mice.

594

595 **Figure 2**

596 **A.** Infrared differential interference contrast optics was used to visualize LCIs (arrows) in WT
597 and symptomatic R6/2 mice. **B-D.** Representative traces of tonic firing of LCIs in the cell-
598 attached configuration. In WTs more LCIs fired action potentials regularly **(B)**. In R6/2s some
599 LCIs fired regularly **(C)** but a greater number of irregular and bursting cells (**D**) were recorded.
600 **E.** High degree of autocorrelation reflected regular firing patterns of LCIs from WT mice. **F.**
601 Although firing of some LCIs from R6/2 animals was highly autocorrelated, the autocorrelation
602 coefficient (peak amplitude or coefficient value of the first lag interval) was lower than in LCIs
603 from WTs. **G.** Low or no autocorrelations were observed in irregular firing and bursting LCIs,
604 particularly from R6/2s. **H.** Spontaneous firing rates in LCIs from WT and R6/2 mice were
605 almost identical. **I.** In contrast, the autocorrelation coefficient, a measure of firing regularity, was
606 significantly decreased in LCIs from R6/2 mice. **J.** Scatter plots showing the correlation between

eNeuro Accepted Manuscript

firing frequency and coefficient of variation. There was a very good correlation between both in LCIs from WT mice. In contrast, this correlation was markedly reduced in cells from R6/2 mice.

**Figure 3**

**A.** Representative traces of spontaneous IPSCs in LCIs from R6/2 and WT mice at 65 days using Cs-Meth or CsCl **(B)** internal solutions. In both cases, spontaneous IPSCs occurred more frequently in LCIs from R6/2 mice. **C.** Amplitude-frequency histograms of sIPSCs using Cs-Meth and CsCl **(D)** internal solutions. In most amplitude bins there was an increase in frequency in LCIs from R6/2 mice. The insets show the mean sIPSC frequency. Regardless of the internal solution used there was a significant increase in LCIs frequency in R6/2s. **E.** Cumulative probability histograms of inter-event intervals in WT and R6/2 mice at 65 days using Cs-Meth and CsCl **(F)** internal solutions. A significant increase in short inter-event intervals was observed in LCIs from R6/2 mice. **G.** Average frequency of miniature (m) IPSCs in LCIs from WT and R6/2 mice was similar using Cs-Meth or CsCl **(H)** internal solutions. The percent reduction in IPSC frequency after TTX was greater in LCIs from R6/2 mice and this difference was statistically significant for the CsCl internal solution (**H**, right panel).

**Figure 4**

**A.** Representative traces of eIPSCs recorded with Cs-Meth internal solution and holding the membrane at +10 mV in LCIs from WT and symptomatic R6/2 mice. eIPSCs had multiple components and amplitude of the earliest peak was measured (arrows). **B.** Graph shows the input-output relationship. Current response amplitudes were significantly increased at intensities of 0.04 mA and higher. **C.** eIPSCs recorded in LCIs at -70 mV with high $Cl^-$ internal solution in

eNeuro Accepted Manuscript

630 WT and R6/2 mice at 65 days. **D.** Similar to recordings with Cs-Meth, there was a significant
631 increase in IPSC amplitudes in cells from R6/2 mice.
632
633 **Figure 5**
634 **A.** Confocal image (z-stack) of a LCI recorded and filled with biocytin (red). The LCI is
635 surrounded by ChR2-EYFP terminals from SOM interneurons (green). Arrows indicate SOM-
636 expressing interneurons. **B.** IPSCs evoked in LCIs by optogenetic stimulation of SOM-
637 expressing interneurons. Responses were significantly larger in LCIs from R6/2 mice. These
638 responses were completely blocked by BIC. **C.** Graphs show significant increases in amplitude
639 and charge in LCIs from R6/2 mice compared to WTs. **D.** LCI surrounded by ChR2-EYFP
640 terminals from PV interneurons. Arrow indicates a PV-expressing interneuron. **E.** IPSCs evoked
641 in LCIs by optogenetic stimulation of PV-expressing interneurons were smaller than those
642 evoked by SOM terminal stimulation and were not different between WT and R6/2 animals.
643 Responses were completely blocked by BIC. **F.** Graphs show the lack of significant differences
644 in peak amplitude and charge in LCIs from WT and R6/2 mice.
645
646 **Figure 6**
647 **A.** Representative traces of eEPSCs in LCIs recorded at -70mV using Cs-Meth internal solution.
648 The peak amplitude of the response was similar in LCIs from WT and R6/2 mice. **B.** Graph
649 shows the input-output relationship of eEPSCs. No statistical differences in amplitude were
650 observed. **C.** Panel shows a striatal LCI (red) surrounded by EYFP terminals in a R6/2 mouse
651 injected with ChR2 in the Cm/Pf nuclear complex. **D.** Optogenetic stimulation of thalamic
652 afferents induced similar AMPA (upper traces) and NMDA (lower traces) receptor-mediated

eNeuro Accepted Manuscript

653 currents in LCIs from WT and R6/2 mice. **E.** Graphs show that the amplitude and charge of
654 AMPA (upper graphs) and NMDA (lower graphs) responses were not significantly different.
655
656 **Figure 7**
657 **A.** Representative traces of responses induced by bath application of increasing concentrations of
658 GABA (10, 100 and 1000 μM) in large striatal neurons (presumably LCIs) from WT and
659 symptomatic R6/2 mice. **B.** Graph shows no significant differences in peak current density (peak
660 current divided by cell capacitance) of GABA responses. **C** and **D.** AMPA- and NMDA-induced
661 peak current densities also were similar in R6/2 and WT mice.
662

eNeuro Accepted Manuscript

663 **References**

664
665
666 Andre VM, Cepeda C, Vinters HV, Huynh M, Mathern GW, Levine MS (2008) Pyramidal cell
667 responses to gamma-aminobutyric acid differ in type I and type II cortical dysplasia. J
668 Neurosci Res 86:3151-3162.

669 Ariano MA, Cepeda C, Calvert CR, Flores-Hernandez J, Hernandez-Echeagaray E, Klapstein
670 GJ, Chandler SH, Aronin N, DiFiglia M, Levine MS (2005) Striatal potassium channel
671 dysfunction in Huntington's disease transgenic mice. J Neurophysiol 93:2565-2574.

672 Bates G, Harper PS, Jones L (2002) Huntington's disease, 3rd Edition. Oxford ; New York:
673 Oxford University Press.

674 Bennett BD, Wilson CJ (1998) Synaptic regulation of action potential timing in neostriatal
675 cholinergic interneurons. J Neurosci 18:8539-8549.

676 Bennett BD, Wilson CJ (1999) Spontaneous activity of neostriatal cholinergic interneurons in
677 vitro. J Neurosci 19:5586-5596.

678 Bennett BD, Callaway JC, Wilson CJ (2000) Intrinsic membrane properties underlying
679 spontaneous tonic firing in neostriatal cholinergic interneurons. J Neurosci 20:8493-8503.

680 Bird ED (1980) Chemical pathology of Huntington's disease. Annu Rev Pharmacol Toxicol
681 20:533-551.

682 Cardin JA, Carlen M, Meletis K, Knoblich U, Zhang F, Deisseroth K, Tsai LH, Moore CI (2009)
683 Driving fast-spiking cells induces gamma rhythm and controls sensory responses. Nature
684 459:663-667.

685 Cepeda C, Wu N, Andre VM, Cummings DM, Levine MS (2007) The corticostriatal pathway in
686 Huntington's disease. Prog Neurobiol 81:253-271.

eNeuro Accepted Manuscript

687 Cepeda C, Itri JN, Flores-Hernandez J, Hurst RS, Calvert CR, Levine MS (2001) Differential
688 sensitivity of medium- and large-sized striatal neurons to NMDA but not kainate receptor
689 activation in the rat. Eur J Neurosci 14:1577-1589.
690 Cepeda C, Chen JY, Wu JY, Fisher RS, Vinters HV, Mathern GW, Levine MS (2014)
691 Pacemaker GABA synaptic activity may contribute to network synchronization in
692 pediatric cortical dysplasia. Neurobiol Dis 62:208-217.
693 Cepeda C, Hurst RS, Calvert CR, Hernandez-Echeagaray E, Nguyen OK, Jocoy E, Christian LJ,
694 Ariano MA, Levine MS (2003) Transient and progressive electrophysiological alterations
695 in the corticostriatal pathway in a mouse model of Huntington's disease. J Neurosci
696 23:961-969.
697 Cepeda C, Starling AJ, Wu N, Nguyen OK, Uzgil B, Soda T, Andre VM, Ariano MA, Levine
698 MS (2004) Increased GABAergic function in mouse models of Huntington's disease:
699 reversal by BDNF. J Neurosci Res 78:855-867.
700 Cepeda C, Galvan L, Holley SM, Rao SP, Andre VM, Botelho EP, Chen JY, Watson JB,
701 Deisseroth K, Levine MS (2013) Multiple sources of striatal inhibition are differentially
702 affected in Huntington's disease mouse models. J Neurosci 33:7393-7406.
703 Chuhma N, Tanaka KF, Hen R, Rayport S (2011) Functional connectome of the striatal medium
704 spiny neuron. J Neurosci 31:1183-1192.
705 Cummings DM, Cepeda C, Levine MS (2010) Alterations in striatal synaptic transmission are
706 consistent across genetic mouse models of Huntington's disease. ASN Neuro 2:e00036.
707 Ding JB, Guzman JN, Peterson JD, Goldberg JA, Surmeier DJ (2010) Thalamic gating of
708 corticostriatal signaling by cholinergic interneurons. Neuron 67:294-307.

eNeuro Accepted Manuscript

709 Farrar AM, Callahan JW, Abercrombie ED (2011) Reduced striatal acetylcholine efflux in the
710 R6/2 mouse model of Huntington's disease: an examination of the role of altered
711 inhibitory and excitatory mechanisms. Exp Neurol 232:119-125.
712 Ferrante RJ, Beal MF, Kowall NW, Richardson EP, Jr., Martin JB (1987) Sparing of
713 acetylcholinesterase-containing striatal neurons in Huntington's disease. Brain Res
714 411:162-166.
715 Ferrante RJ, Kowall NW, Beal MF, Richardson EP, Jr., Bird ED, Martin JB (1985) Selective
716 sparing of a class of striatal neurons in Huntington's disease. Science 230:561-563.
717 Fusco FR, Chen Q, Lamoreaux WJ, Figueredo-Cardenas G, Jiao Y, Coffman JA, Surmeier DJ,
718 Honig MG, Carlock LR, Reiner A (1999) Cellular localization of huntingtin in striatal
719 and cortical neurons in rats: lack of correlation with neuronal vulnerability in
720 Huntington's disease. J Neurosci 19:1189-1202.
721 Gonzales KK, Pare JF, Wichmann T, Smith Y (2013) GABAergic inputs from direct and indirect
722 striatal projection neurons onto cholinergic interneurons in the primate putamen. J Comp
723 Neurol 521:2502-2522.
724 Graybiel AM (1990) Neurotransmitters and neuromodulators in the basal ganglia. Trends
725 Neurosci 13:244-254.
726 Graybiel AM (1995) Building action repertoires: memory and learning functions of the basal
727 ganglia. Curr Opin Neurobiol 5:733-741.
728 Gundersen HJ, Jensen EB (1987) The efficiency of systematic sampling in stereology and its
729 prediction. J Microsc 147:229-263.

eNeuro Accepted Manuscript

730 Klapstein GJ, Fisher RS, Zanjani H, Cepeda C, Jokel ES, Chesselet MF, Levine MS (2001)
731 Electrophysiological and Morphological Changes in Striatal Spiny Neurons in R6/2
732 Huntington's Disease Transgenic Mice. J Neurophysiol 86:2667-2677.
733 Kosinski CM, Cha JH, Young AB, Mangiarini L, Bates G, Schiefer J, Schwarz M (1999)
734 Intranuclear inclusions in subtypes of striatal neurons in Huntington's disease transgenic
735 mice. Neuroreport 10:3891-3896.
736 Lapper SR, Bolam JP (1992) Input from the frontal cortex and the parafascicular nucleus to
737 cholinergic interneurons in the dorsal striatum of the rat. Neuroscience 51:533-545.
738 Levine MS, Klapstein GJ, Koppel A, Gruen E, Cepeda C, Vargas ME, Jokel ES, Carpenter EM,
739 Zanjani H, Hurst RS, Efstratiadis A, Zeitlin S, Chesselet MF (1999) Enhanced sensitivity
740 to N-methyl-D-aspartate receptor activation in transgenic and knockin mouse models of
741 Huntington's disease. J Neurosci Res 58:515-532.
742 Mangiarini L, Sathasivam K, Seller M, Cozens B, Harper A, Hetherington C, Lawton M, Trottier
743 Y, Lehrach H, Davies SW, Bates GP (1996) Exon 1 of the HD gene with an expanded
744 CAG repeat is sufficient to cause a progressive neurological phenotype in transgenic
745 mice. Cell 87:493-506.
746 Martone ME, Armstrong DM, Young SJ, Groves PM (1992) Ultrastructural examination of
747 enkephalin and substance P input to cholinergic neurons within the rat neostriatum. Brain
748 Res 594:253-262.
749 Meade CA, Deng YP, Fusco FR, Del Mar N, Hersch S, Goldowitz D, Reiner A (2002) Cellular
750 localization and development of neuronal intranuclear inclusions in striatal and cortical
751 neurons in R6/2 transgenic mice. J Comp Neurol 449:241-269.

eNeuro Accepted Manuscript

752 Pakhotin P, Bracci E (2007) Cholinergic interneurons control the excitatory input to the striatum.
753 J Neurosci 27:391-400.
754 Picconi B, Passino E, Sgobio C, Bonsi P, Barone I, Ghiglieri V, Pisani A, Bernardi G,
755 Ammassari-Teule M, Calabresi P (2006) Plastic and behavioral abnormalities in
756 experimental Huntington's disease: a crucial role for cholinergic interneurons. Neurobiol
757 Dis 22:143-152.
758 Pisani A, Bernardi G, Ding J, Surmeier DJ (2007) Re-emergence of striatal cholinergic
759 interneurons in movement disorders. Trends Neurosci 30:545-553.
760 Reiner A, Albin RL, Anderson KD, D'Amato CJ, Penney JB, Young AB (1988) Differential loss
761 of striatal projection neurons in Huntington disease. Proc Natl Acad Sci U S A 85:5733-
762 5737.
763 Reiner A, Shelby E, Wang H, Demarch Z, Deng Y, Guley NH, Hogg V, Roxburgh R, Tippett LJ,
764 Waldvogel HJ, Faull RL (2013) Striatal parvalbuminergic neurons are lost in
765 Huntington's disease: implications for dystonia. Mov Disord 28:1691-1699.
766 Sadikot AF, Parent A, Francois C (1992) Efferent connections of the centromedian and
767 parafascicular thalamic nuclei in the squirrel monkey: a PHA-L study of subcortical
768 projections. J Comp Neurol 315:137-159.
769 Smith R, Chung H, Rundquist S, Maat-Schieman ML, Colgan L, Englund E, Liu YJ, Roos RA,
770 Faull RL, Brundin P, Li JY (2006) Cholinergic neuronal defect without cell loss in
771 Huntington's disease. Hum Mol Genet 15:3119-3131.
772 Smith TK, McCarron SL (1998) Nitric oxide modulates cholinergic reflex pathways to the
773 longitudinal and circular muscle in the isolated guinea-pig distal colon. J Physiol 512 ( Pt
774 3):893-906.

eNeuro Accepted Manuscript

775 Sohal VS, Zhang F, Yizhar O, Deisseroth K (2009) Parvalbumin neurons and gamma rhythms
776 enhance cortical circuit performance. Nature 459:698-702.
777 Sullivan MA, Chen H, Morikawa H (2008) Recurrent inhibitory network among striatal
778 cholinergic interneurons. J Neurosci 28:8682-8690.
779 Szydlowski SN, Pollak Dorocic I, Planert H, Carlen M, Meletis K, Silberberg G (2013) Target
780 selectivity of feedforward inhibition by striatal fast-spiking interneurons. J Neurosci
781 33:1678-1683.
782 Tong X, Ao Y, Faas GC, Nwaobi SE, Xu J, Haustein MD, Anderson MA, Mody I, Olsen ML,
783 Sofroniew MV, Khakh BS (2014) Astrocyte Kir4.1 ion channel deficits contribute to
784 neuronal dysfunction in Huntington's disease model mice. Nat Neurosci.
785 Vetter JM, Jehle T, Heinemeyer J, Franz P, Behrens PF, Jackisch R, Landwehrmeyer GB,
786 Feuerstein TJ (2003) Mice transgenic for exon 1 of Huntington's disease: properties of
787 cholinergic and dopaminergic pre-synaptic function in the striatum. J Neurochem
788 85:1054-1063.
789 Vonsattel JP, DiFiglia M (1998) Huntington disease. J Neuropathol Exp Neurol 57:369-384.
790 Won L, Ding Y, Singh P, Kang UJ (2014) Striatal cholinergic cell ablation attenuates L-DOPA
791 induced dyskinesia in Parkinsonian mice. J Neurosci 34:3090-3094.
792
793

eNeuro Accepted Manuscript

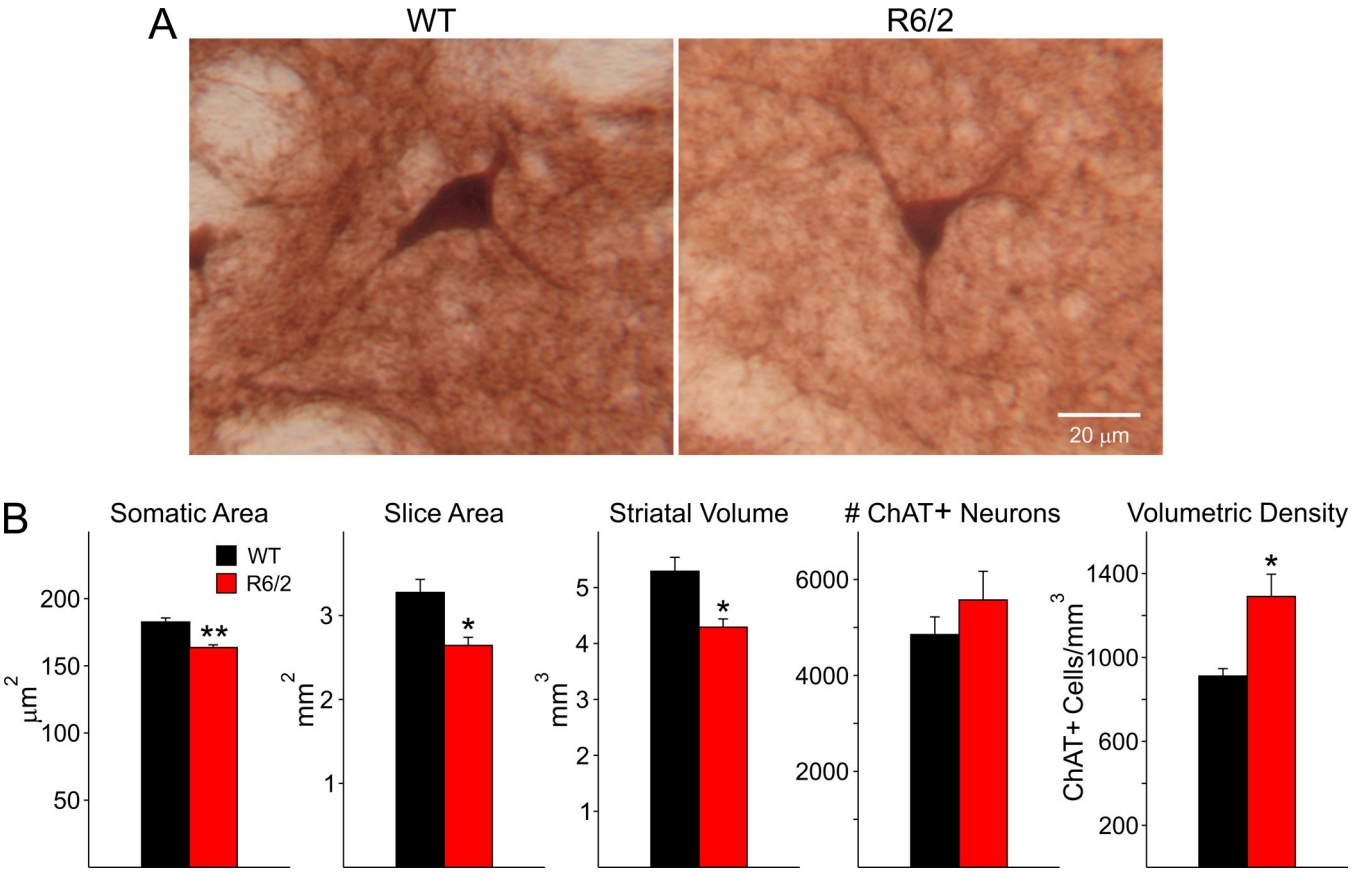

eNeuro Accepted Manuscript

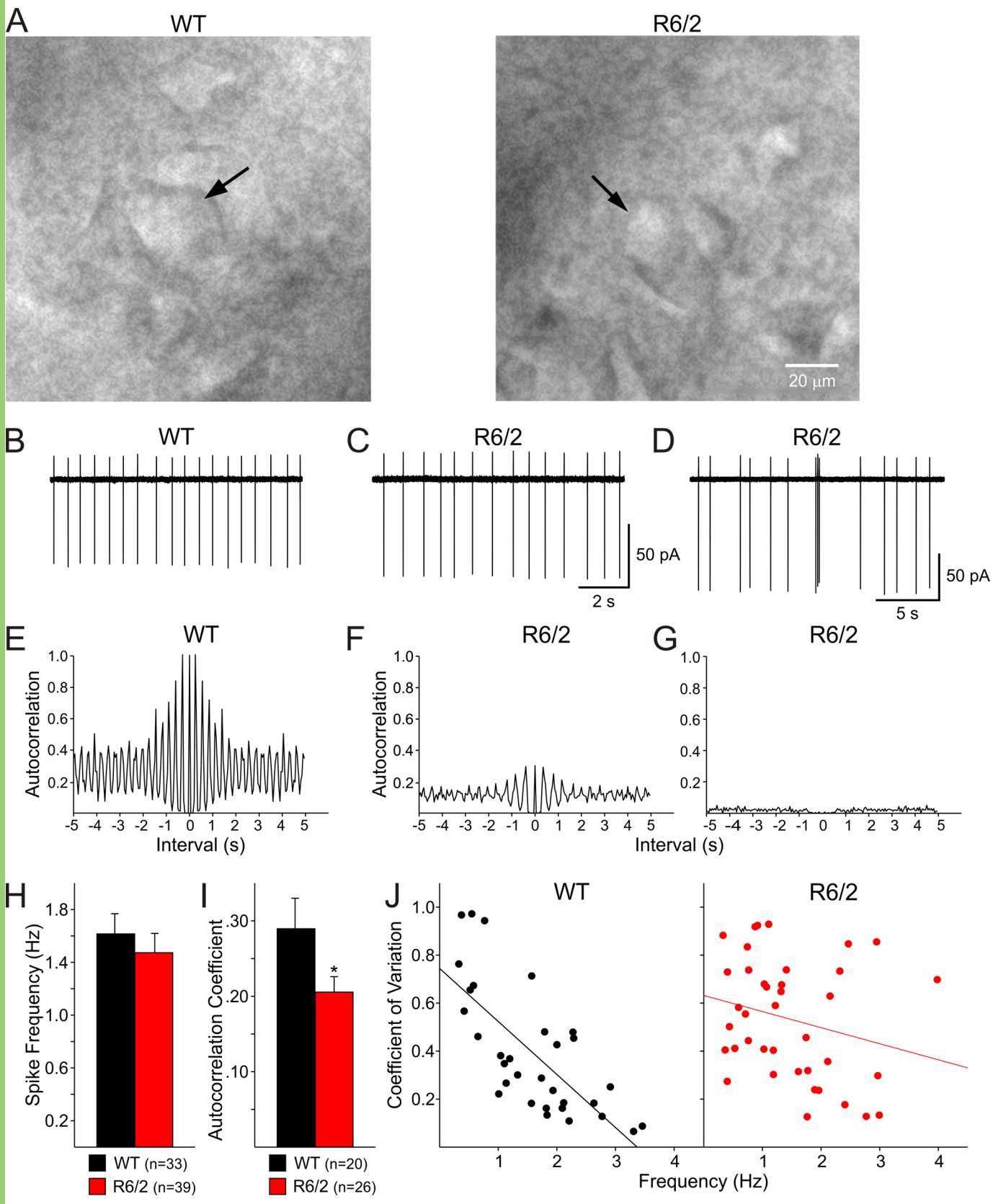

eNeuro Accepted Manuscript

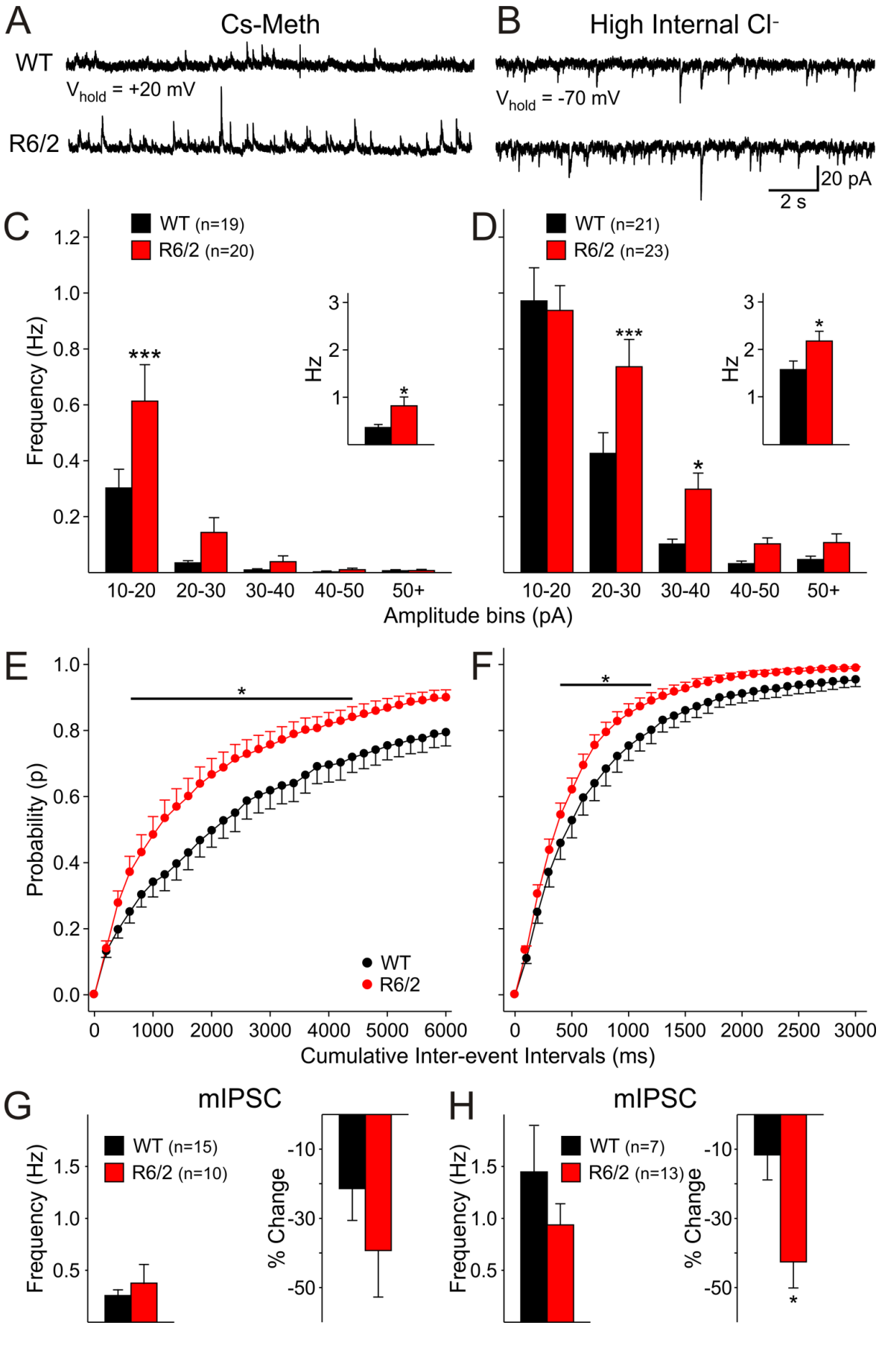

eNeuro Accepted Manuscript

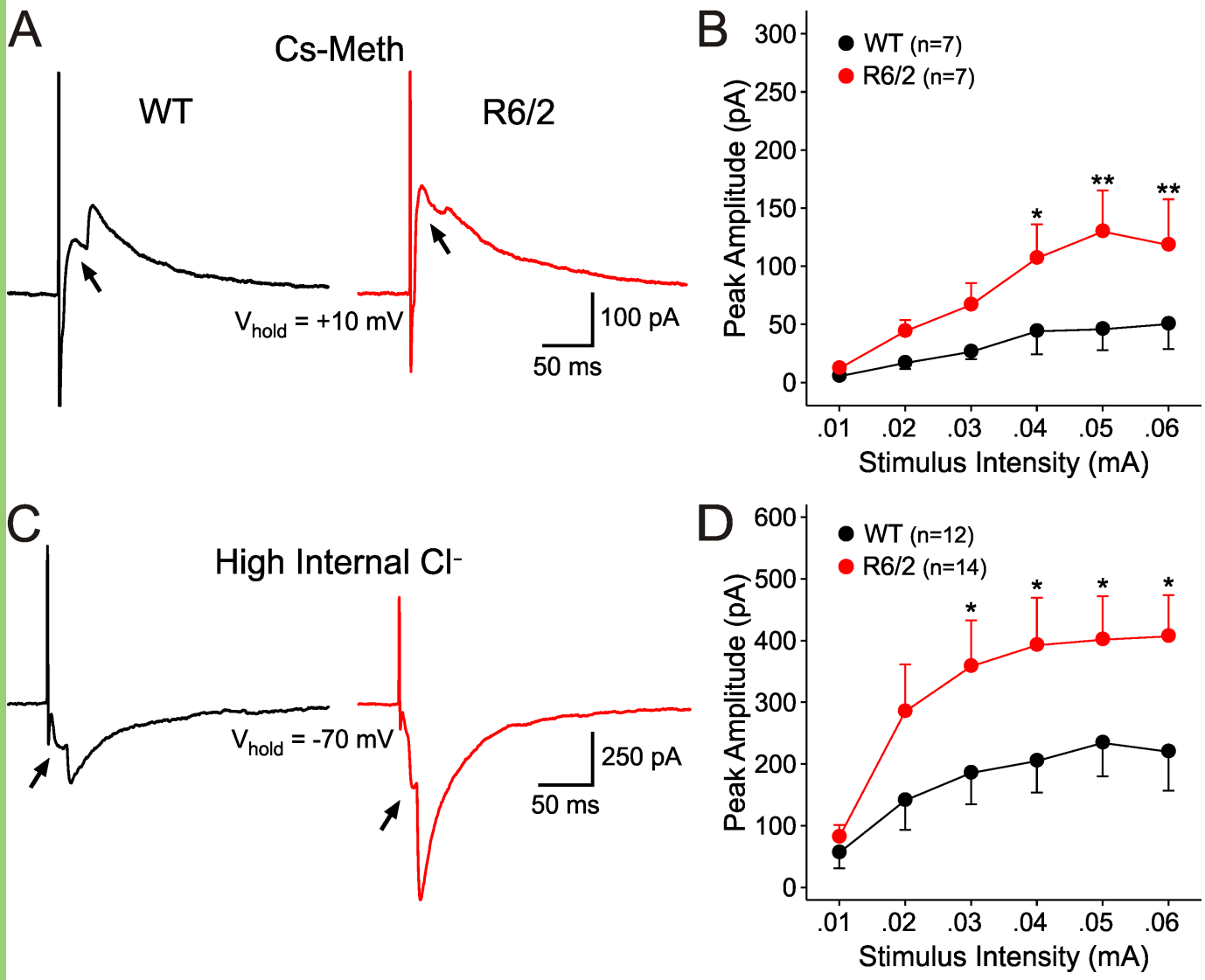

eNeuro Accepted Manuscript

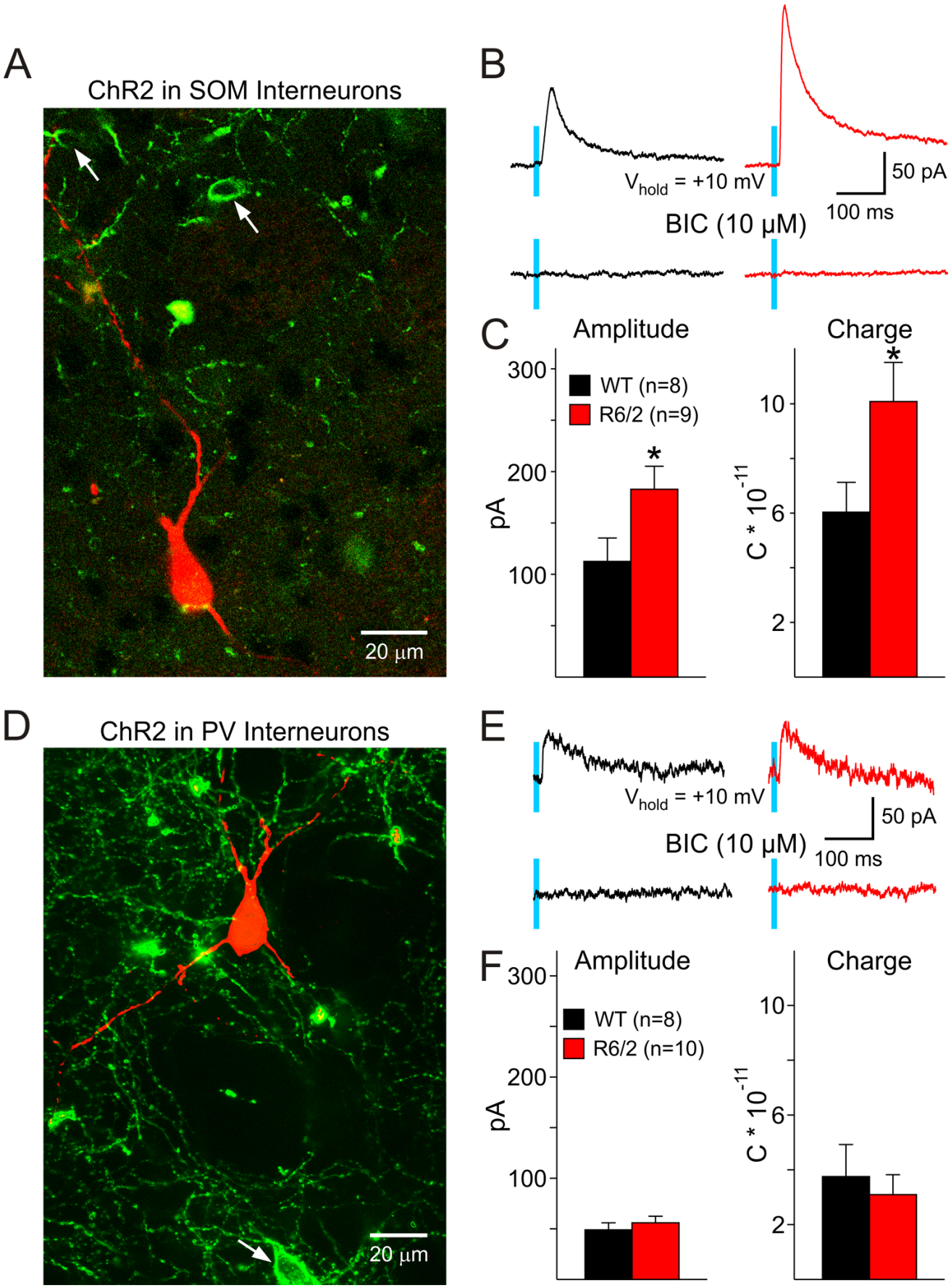

eNeuro Accepted Manuscript

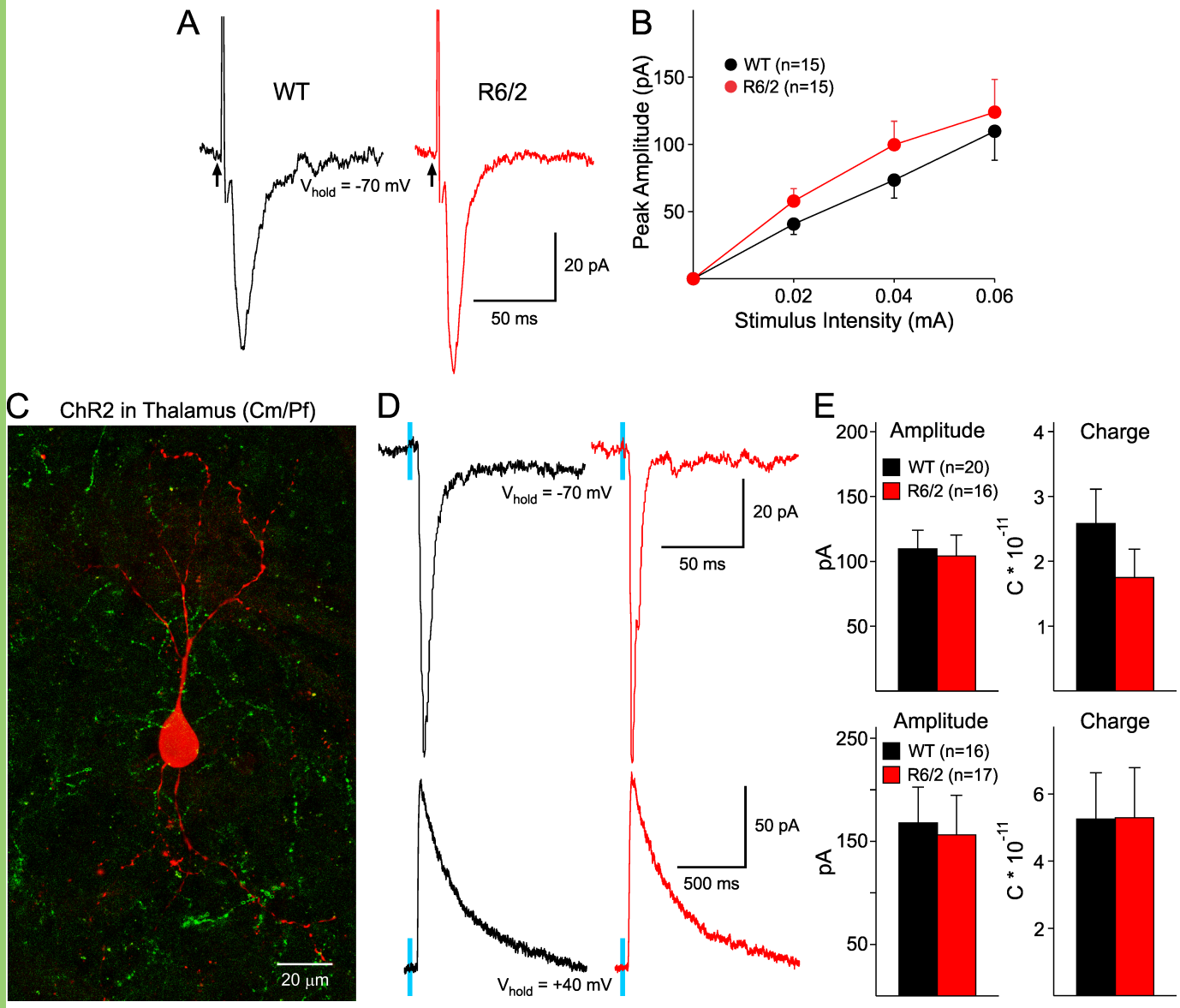
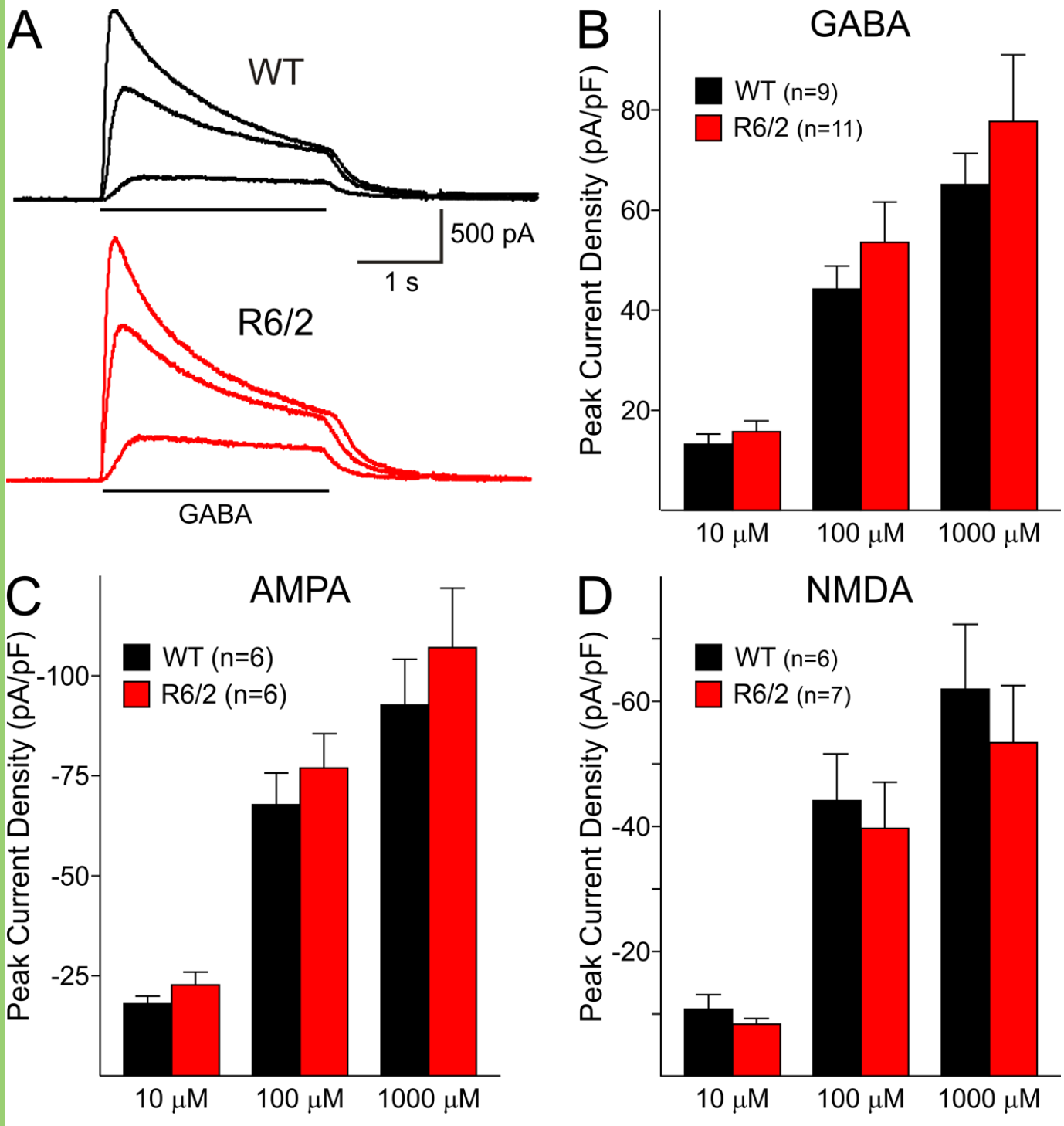
eNeuro Accepted Manuscript